Article

Design and Realization of a Multiple Access Wireless Power Transfer System for Optimal Power Line Communication Data Transfer

Sami Barmada [1,*,†] , Mauro Tucci [1,†] , Nunzia Fontana [1,†] and Wael Dghais [2,†] and Marco Raugi [1,†]

1   Department of Energy, Systems, Territory and Construction Engineering, University of Pisa, 56122 Pisa, Italy; mauro.tucci@unipi.it (M.T.); nunzia.fontana@unipi.it (N.F.); marco.raugi@unipi.it (M.R.)
2   Department of Electronics, Higher Institute of Applied Science and Technology of Sousse, Université de Sousse, Sousse 4003, Tunisia; waeldghais@ua.pt
*   Correspondence: sami.barmada@unipi.it; Tel.: +39-050-221-7312
†   These authors contributed equally to this work.

check for updates

Abstract: In this contribution, the authors evaluate the possibility of using separated access points for power and data transfer in a coupled Wireless Power Transfer-Powerline Communication system. Such a system has been previously proposed by the authors for specific applications, in which Wireless Power Transfer (WPT) should take place in a system where data are transmitted over the power grid. In previous works the authors have performed lab tests on a two coils WPT system equipped with a set of filters to also allow an efficient data transfer. When a multiple coil WPT system is chosen, additional possibilities arise: the access point for power and data can be differentiated, with the aim of maintaining the designed power efficiency and increase data transfer capacity. In this study a four coils WPT system is thoroughly analyzed, modelled, implemented and measured, and a set of guidelines for the correct design (in terms of performance optimization) of the data transfer is given.

Keywords: wireless power transfer; power line communications; channel characterization

1. Introduction

Wireless Power Transfer (WPT) technology has lately gained increasing attention as an alternative way to transmit power with respect to a cabled connection, see for instance [1–3]. In particular, applications for small portable consumer electronic devices are already available on the market (i.e., cellular phones, electric tooth brushes and the Qi standard, etc.) while high power applications are still the object of research, study and prototyping (charging of electric vehicles or hybrid vehicles is an example). In the last decade, Power Line Communication (PLC) has been recognised as a viable option for broadband communications, and it can compete with other, and more diffused, technologies when operating in specific environments. PLC technology uses power cables to transmit high speed data; in fact it uses the power grid, that is designed to carry voltages and currents at the mains frequency (typically at 50/60 Hz) to transmit data at much higher frequencies, that are now up to a tenth of MHz, in the most common commercial products. Domestic applications of PLC technology are quite widely diffused, while, on a larger scale, PLC communication is now considered one of the main possibilities to transmit data in a smart grid environment (when, for instance, long distances do not allow wireless data transmission). Recently, the PLC technology has been proposed to substitute part of the cable harness in electric vehicles [4–6]. These two technologies are apparently colliding, since WPT transfers power wirelessly while PLC transmits data on a cabled connection originally

designed for power. This has led the authors to the idea that a full integration between WPT and PLC could be a solution allowing the use of WPT without the need for changes to a pre-existing PLC system. In [7] a feasibility study of such a system is proposed, in which a preliminary logic outline of the whole system is shown, and the evaluation of the available channel capacity is performed based on a typical four-coils system. In [8], an optimization procedure performed on the lumped equivalent circuit is presented, showing that such a system can be properly designed taking into account both power and data transmission requirements. In addition, in [9] the full system (with coils and filters) was designed and built showing the actual feasibility of the proposal; in particular, ref. [9] is specifically referring to a two-coils WPT system.

In this contribution the authors investigate for the first time the possibility of using the loops and the coils (respectively called also "outer coils" and "inner coils") of a four coils system as different access points: while the power generator and load are respectively connected to the drive and load loop, the data modems are now connected between the coils. This completely new concept, under specific circumstances, can guarantee a wider communication band, hence better communication performances.

In [9], the two coils system has been designed to transmit power at the resonant frequency of $f_0 = 6.78$ MHz, that is often related to low power applications such as energy harvesting devices etc., see for instance [10] . In this paper the system is designed to transmit power at a frequency of hundreds of kHz, typical of high power applications such as battery charging of electric vehicles, as shown in [11]. In addition, the frequency range considered in this paper is typical of narrow band (NB) PLC, in contrast to broad band PLC that uses tens of MHz. Then, this work shows for the first time that NB-PLC and WPT can coexist and share the same medium. The proposed system is of great potential and can be the key point in which both data and power should be transferred, for instance in a Battery Management System for electric vehicles [12] or in domestic applications [13]. The paper is organized as follows: in Section 2 the rationale behind the main idea is described; in Section 3 it is described how the system has been built according to analytical relations; in Section 4 the theoretical analysis relative to the optimal relation between resonant frequency, distance and load is obtained, while Section 5 presents the analytical and theoretical results for the proposed system.

2. WPT System with Multiple Data Access

Figure 1 shows the typical equivalent circuit of the non radiative four coils WPT system with the so called drive and load loops (where the source and the load are connected) and the transmitting and receiving coils, that are basically used as repeaters in order to increase the power transmission distance (reducing k_{23}) retaining maximum power transfer. The inductances L_2 and L_3 represent the transmitting and receiving coils, while L_1 and L_4 represent the drive loop and load loop inductors respectively. The resistances $R_{pj}, j = \{1, 2, 3, 4\}$ represent the winding resistances of the corresponding inductor and are, as a matter of fact, parasitic elements. The mutual inductance $M_{ij} = k_{ij}\sqrt{L_i L_j}$ represents the coupling between the inductors L_i and L_j (with coupling coefficient k_{ij}), while the capacitors $C_j, j = \{1, 2, 3, 4\}$ are designed to resonate with the corresponding inductor at the resonance frequency. The coupling factor k_{23} depends on the distance between the transmitting and receiving coils, which is a fundamental design parameter. In this scheme, parasitic capacitances (basically given by the turn to turn capacitance of each inductor) are not represented, since they are grouped together with the capacitances C_j (of each inductor). Usually the transmitting and receiving coil (also called "inner coils" due to the fact that are represented in between the other two inductors) have no access point and are often mounted on the same equipment as the relative loop.

The use of a lumped equivalent circuit to represent a WPT system is a common way to understand and design it; speaking of frequencies in the range of kHz to few MHz, we are in the field of non radiative WPT systems, and this approach will be used throughout the paper.

When additional data transfer capabilities (with the motivation of interfacing to a PLC system) have been added to the WPT system, the most logical approach was to use the same terminals of

the power transfer: this is trivial for a two-coils system, and was the first choice for a four-coils system ([7–9]).
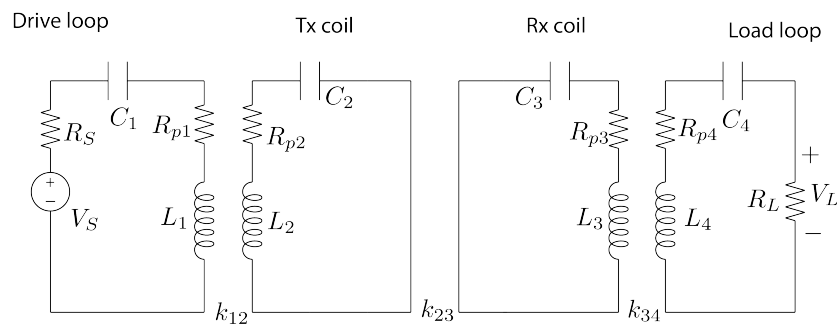

Figure 1. Four coils lumped equivalent circuit.

A first theoretical study regarding the use of different access points for four-coils WPT systems has been performed in [14]: two different circuits have been analyzed as shown in Figures 2 and 3. The circuit of Figure 1 has been modified in order to include additional filters that are actually required in the proposed combined system WPT-PLC: they should prevent power from flowing through the PLC modem (to avoid damages) and guarantee optimal coupling between the modem and the WPT system, possibly not affecting the power channel in terms of efficiency.
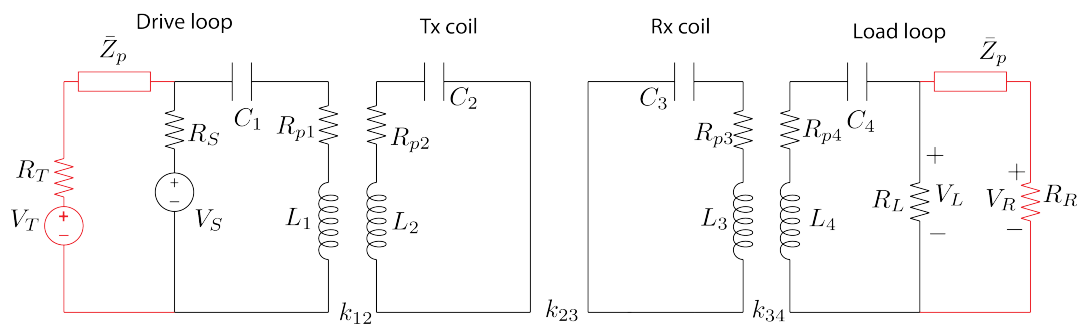

Figure 2. Power and data from the outer coils, with the inclusion of the parallel filter.

The system in Figure 2 is basically the one described in [9], with the parallel resonant circuit $\bar{Z}_p$ that resonates at the frequency of the power signal, hence operating as an open circuit. In this way the power signal (generated by V_S and received by R_L) does not flow into the PLC modem V_T. On the contrary, the wideband data signal generated by V_T and received by R_R is not affected by the higher magnitude power signal.
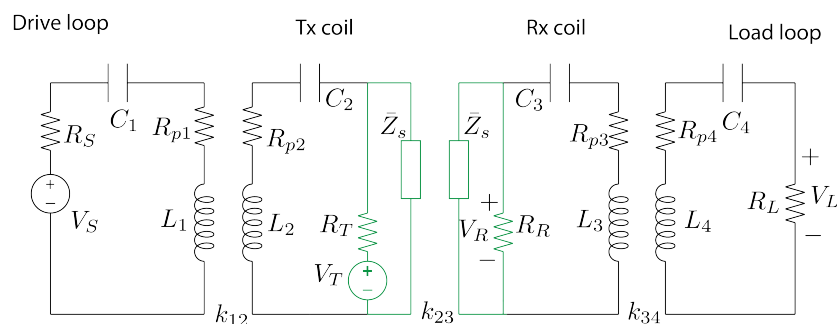

Figure 3. Data from the inner coils, with the inclusion of the series filter.

Figure 3 shows the new architecture object of this theoretical and practical study: data communication is performed between the inner coils, with the addition of the $\bar{Z}_s$ series resonant circuit; this series LC filter behaves as a short circuit at the power frequency, basically eliminating

from the inner loops the modem and the transmitting and receiving loads (respectively V_T, R_R,R_T): in this way the power signal does not flow through the PLC modem and it is not dissipated into the receiving and transmitting resistances. At frequencies different from f_0, data signal can flow between the inner coils.

In this paper the authors have considered, for the sake of simplicity, second order parallel or series LC resonant circuits resonating at the power frequency f_0. Despite the simplicity of this approach, the results obtained clearly indicate that good performances can be achieved. Given the equivalent circuits shown above, it is possible to derive the analytical transfer functions both for power and data transfer: Equations (A1) and (A2) are relative to the transfer function of the power channel of the circuit in Figure 2, while (A3) and (A4) are relative to the transfer function of the data channel in the same circuit. In the same way, Equations (A5) and (A6) are relative to the transfer function of the power channel of the circuit in Figure 3, while (A7) and (A8) are relative to transfer function of the data channel in the same circuit. These expressions will be used in Section 5 and compared with experimental results.

In [14] a theoretical analysis has been performed on the two circuits with a specific set of circuit's parameters values (which were originally given in [15]); these theoretical results show that, in this specific case, the channel capacity in terms of bit rate is higher when data is transmitted between the inner coils. Far from being an exhaustive analysis, these results have led the authors to perform additional investigations and experimental validation, that are reported in this paper.

3. Coil Design

The design of the WPT system has been performed taking into account the working frequencies and coils dimensions, allowing a simple experimental setup. In four coils WPT systems, the loop (e.g., power access point) and the short circuited coil are a unique system in which their mutual distance is kept as constant; in most cases, two twin loop-coil system are used to create a four coils WPT system.

Figure 4 shows the outline of a loop-coils set, in which the dimensions are relative to the coils support and are reported in Table 1.
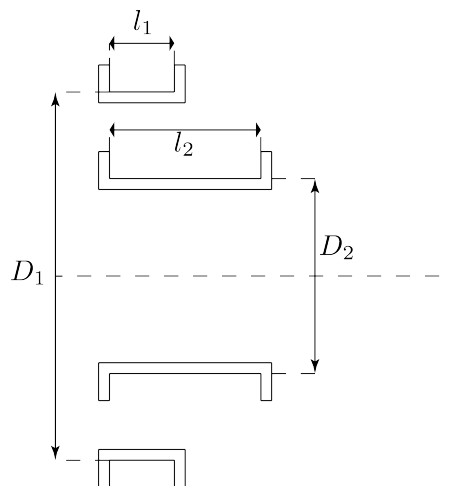

Figure 4. Axial section of a loop-coil set.

Table 1. Dimensions of the coils support.

	Diameter	Length
Loop	$D_1 = 18$ cm	$l_1 = 2$ cm
Coil	$D_2 = 12$ cm	$l_2 = 8$ cm

In order to reduce the resistance due to skin and proximity effect, a copper Litz wire has been used: the chosen wire is characterized by 600 strands, each of them having a diameter of 0.1 mm;

considering that skin depth at the frequency $f = 1$ MHz is about 65 µm, the chosen wire works well for power frequencies of the order of a few MHz. The coils have been realized as single layer coils, whose value of self inductance has been calculated according to [16] and the self capacitance according to [17]; these values are reported in Table 2.

Table 2. Electrical parameters of the inductors.

	Turns	Self Inductance	Self Capacitance
Loop	$N_1 = 5$	$L_1 = 8.68\,µH$	$C_{p1} = 21.57\,pF$
Coil	$N_2 = 19$	$L_2 = 40.93\,µH$	$C_{p2} = 30.20\,pF$

The coupling coefficient (hence the mutual inductance) for the configuration shown in Figure 4 has been consequently calculated according to [18], resulting in the following values: $M_{12} = 6.70\,µH$, $k_{12} = 0.3711$.

The four coils system is composed by two loop-coil sets facing each other; the coupling coefficient k_{23} between the two coils have been calculated for distances varying in the range between 3 cm and 23 cm ([18]); some of them are reported in Table 3. It is worth noting that the coupling between loop and coil belonging to different sets (i.e., k_{13} and k_{24}) have been neglected, as it is usually done in such cases. This assumption is justified by analyzing the distance between the left loop and the right coil (considering the dimensions shown in Figure 4) and the results in Table 3: k_{13} and k_{24} would be much lower than the other coefficients.

Table 3. Coupling coefficient k_{23} of the coils as a function of the distance.

Distance (cm)	5	7	11	15	19	23
Coupling coefficient k_{23}	0.0891	0.0614	0.0321	0.0189	0.0114	0.0077

In order to validate the design procedure, the self inductances have been measured with a Vector Network Analyser (VNA) which allows verifying the frequency behavior of the system as well. The measured values of the inductances are $L_1 = 9.2\,µH$ and $L_2 = 43.8\,µH$ showing a good agreement with the design parameters which are listed in Table 2. The AC resistance of the coils were also measured, obtaining $R_{p1} = 6\,mΩ$ and $R_{p2} = 24\,mΩ$. The setup of Figure 4 has been experimentally implemented as depicted in Figure 5 and the two coils have been connected to the two ports of the VNA, measuring the frequency behavior of the scattering parameter S_{21} (also called transmission coefficient). Figure 6 shows the comparison between measurement and analytical calculations (not reported here for a two coils system for the sake of conciseness): as described, the system realized matches with very good accuracy the design criteria.
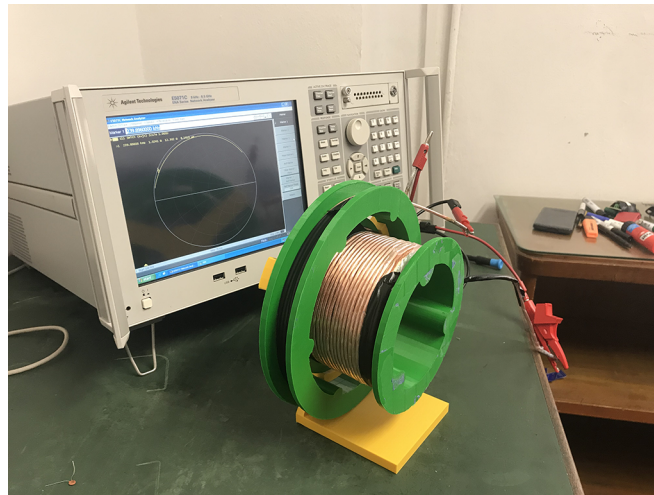
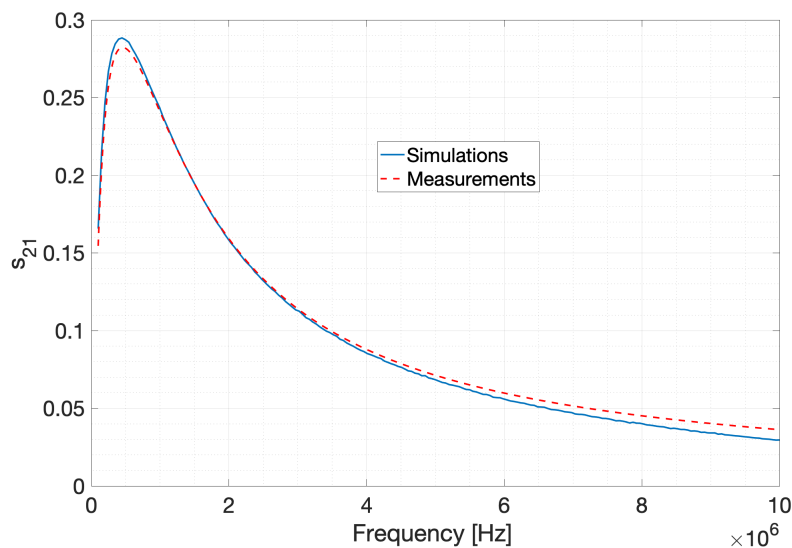**Figure 5.** Experimental characterization and validation of the setup.

Figure 6. S_{21} scattering parameter relative to the coil-loop system.

4. Four-Coils WPT Input Impedance System Modeling

This section focuses on the modeling of a four coils WPT system, in particular we first recall the equations of the circuit, then we derive an exact analytical expression of the input impedance of the four coils system at the resonance frequency. To the authors' knowledge, the expression of the input impedance so obtained is slightly different with respect to the ones derived in the literature, and it allows to design the WPT system to accomplish maximum power transfer. A four-coils WPT system is shown in Figure 7. The equations using the mesh analysis are as follows:

$$\begin{cases} \dot{E} = \left(R_S + R_{p1} + j\omega L_1 + \frac{1}{j\omega C_1} \right) \dot{I}_1 + j\omega M_{12} \dot{I}_2 \\ 0 = j\omega M_{12} \dot{I}_1 + \left(R_{p2} + j\omega L_2 + \frac{1}{j\omega C_2} \right) \dot{I}_2 + j\omega M_{23} \dot{I}_3 \\ 0 = j\omega M_{23} \dot{I}_2 + \left(R_{p3} + j\omega L_3 + \frac{1}{j\omega C_3} \right) \dot{I}_3 + j\omega M_{34} \dot{I}_4 \\ 0 = j\omega M_{34} \dot{I}_3 + \left(R_L + R_{p4} + j\omega L_4 + \frac{1}{j\omega C_4} \right) \dot{I}_4 \end{cases} \quad (1)$$
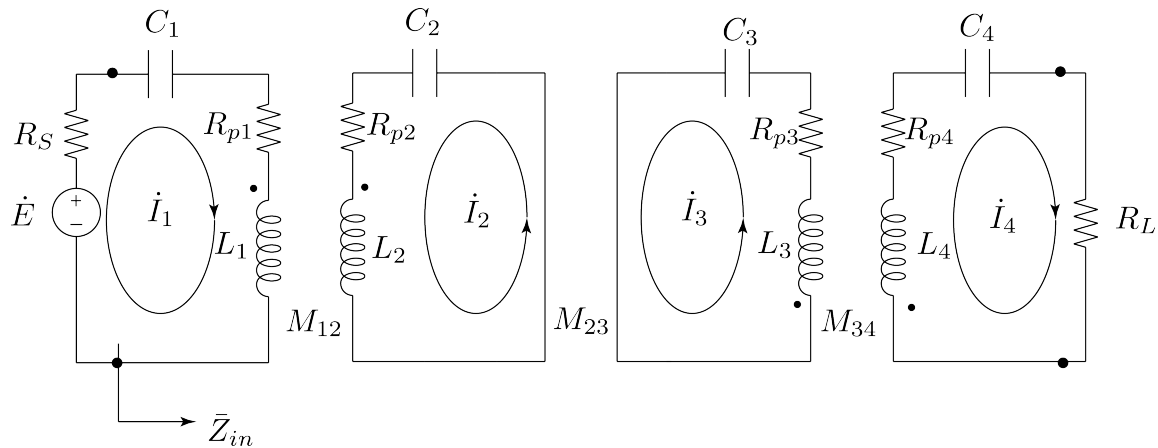
Figure 7. Four-coils Wireless Power Transfer (WPT) system.

At the resonant angular frequency ω_0, considering that $\omega_0 L_k = \frac{1}{\omega_0 C_k}$, and neglecting the parasitic resistances $R_{pj}, j = \{1, 2, 3, 4\}$, equations in (1) become

$$
\begin{cases}
\dot{E} = R_S \dot{I}_1 + j\omega_0 M_{12} \dot{I}_2 \\
0 = j\omega_0 M_{12} \dot{I}_1 + j\omega_0 M_{23} \dot{I}_3 \\
0 = j\omega_0 M_{23} \dot{I}_2 + j\omega_0 M_{34} \dot{I}_4 \\
0 = j\omega_0 M_{34} \dot{I}_3 + R_L \dot{I}_4
\end{cases}
\tag{2}
$$

From Equation (2) it is straightforward to derive the input impedance $\bar{Z}_{in}$:

$$
\bar{Z}_{in} = \left(\omega_0 \frac{M_{12} M_{34}}{M_{23}} \right)^2 \frac{1}{R_L}.
\tag{3}
$$

We note that the impedance is real, and it can be written in terms of the coupling coefficients as

$$
\bar{Z}_{in} = \left(\omega_0 \frac{k_{12} k_{34}}{k_{23}} \right)^2 \frac{L_1 L_4}{R_L}.
\tag{4}
$$

Knowing the exact expression of the input impedance at the resonance frequency allows us to design the system in order to achieve maximum power transfer, by placing

$$
\bar{Z}_{in} = R_S.
\tag{5}
$$

It is interesting to compare our result with the one reported in [19], where parallel resonant capacitors were used in the drive loops, and where the maximum power transfer condition was shown to be met if $k_{12} k_{34} = k_{23}$. The latter result was obtained by neglecting the parasitic resistances, as in our case, but also neglecting the parallel capacitor in the transmitting drive loop, which was considered as open circuit. On the contrary, our result is exact, and it allows an optimal matching. Moreover Equations (4) and (5) bring new design guidelines, that highlight a dependence between the optimal resonant frequency and the coupling coefficient k_{23}:

$$
\omega_0 = \frac{k_{23}}{k_{12} k_{34}} \sqrt{\frac{R_L R_S}{L_1 L_4}}
\tag{6}
$$

In order to design the system we used Equation (6), where the only free parameter is k_{23} as it depends on the distance between coils as shown in Table 3. After having designed, as in the previous section, the coils dimensions and geometries (determining the coupling coefficients k_{12}, k_{34}, and the inductances) the next design steps are as follows:

- select the distance between coils;
- determine the corresponding coupling coefficient k_{23} as in Table 3;
- determine the optimal resonance frequency from Equation (6);
- design the resonant capacitors as $C_k = \frac{1}{\omega_0^2 L_k}$ for $k = 1 \ldots 4$.

It is noteworthy that the expression shown in 4 is valid for any load, since it is sufficient to substitute the resistance R_L with the load impedance $\bar{Z}_L$. There are many papers related to the evaluation of the load impedance depending on the power electronics receiving the high frequency a.c. power. The use of a resistive load R_L in this paper does not change the rationale behind the idea and it is an approximation that is generally used.

5. Theoretical and Experimental Results

5.1. Description of the Measurement Setup

The WPT system has been implemented and a measurement campaign has been performed to verify the theoretical results; a photo of the whole system composed by the four coils (assembled in the form of two coil-loop subsystems), the filters and the VNA is shown in Figure 8.
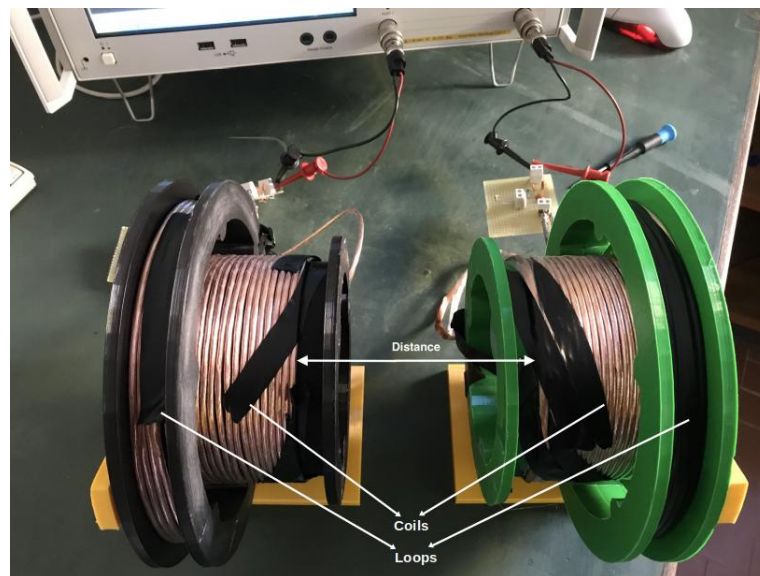

Figure 8. WPT system during measurement.

The theoretical results showing that the inner coils can be chosen as data access point in order to increase bandwidth are experimentally verified; in particular we realized two test cases for two different distances, namely 5 cm and 15 cm. The corresponding resonant frequencies and capacitors values are shown in Table 4.

Table 4. Test case configurations.

Parameter	Case Study 1	Case Study 2
Distance	5 (cm)	15 (cm)
Coupling coefficient k_{23}	0.0891	0.0189
Resonant frequency f_0	578.2 kHz	122.6 kHz
Capacitors C_1 and C_4	8.27 nF	184 nF
Capacitors C_2 and C_3	1.72 nF	38.3 nF

For each case, the series and parallel filters ($\bar{Z}_s$ and $\bar{Z}p$) have been realized as ideal second order series or parallel $L - C$ circuits; from the theoretical calculations (with the analytical expressions

presented in the Appendix A), we have verified that the proper selection of the data access point is strictly influenced by the filter design; in particular, considering that all the filters must resonate at the chosen frequency f_0, there is a degree of freedom in the choice of the inductor or the capacitor. In order to highlight the different behavior, the authors report here two different choices for each case study:

(a) The *LC* filter is constructed with *L* and *C* components whose values are coincident to the values of *L* and *C* of the inductor it is connected to. For instance, the filter $\bar{Z}_p$ connected to the drive loop 1 having inductance equal to L_1 and capacitance C_1 is realized with components $L_p = L_1$ and $C_P = C_1$; the same holds for the series filter $\bar{Z}_s$.

(b) The *LC* filter is constructed with *L* and *C* components whose values are coincident the values of *L* and *C* of the inductor they are not connected to. For instance, the filter $\bar{Z}_p$ connected to the drive loop 1 is realized with components $L_p = L_2$ and $C_P = C_2$; the same holds for the series filter $\bar{Z}_s$.

As it will be shown later, these two choices lead to different behavior of the data channel. It must be pointed out that the simulation results shown in this section have been obtained using for L_1, L_2, L_3 and L_4 the measured values (and not the design values) given in Section 3.

5.2. Case Study 1 (Distance 5 cm)

For Case Study 1, the following table resumes the filter parameters for the subcases (a) and (b); in all the figures reported in this section, the transfer function has been taken as output; when the power channel is considered, in order to obtain the scattering parameter S_{21} it is sufficient to multiply by 2 the transfer function V_L/V_S since the circuit works with the termination resistances of $50\,\Omega$ of the VNA, according to

$$S_{21} = 2\sqrt{\frac{R_S}{R_L}}\frac{V_L}{V_S} \tag{7}$$

Figure 9 shows the comparison between the analytical calculations and measurements for the power channel in Case Study 1a; in particular Figure 9 is referred to the data access from the outer coils (the system represented in Figure 2), and the values of the filters as reported in Table 5. While from the design results at the resonant frequency the power transfer should achieve an efficiency close to unity (where efficiency is referred to as power transfer efficiency and not frequency efficiency), measurements shows a decrease of about 10%: this is due to the components' tolerance and parasitic effects. For instance, the parallel *LC* filter does not behave exactly as an ideal filter; however, the design frequency is reasonably achieved, together with a good maximum value of S_{21}.
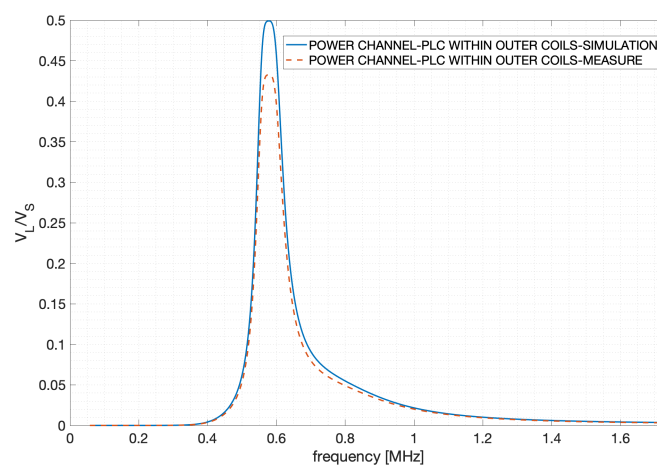

Figure 9. Transfer functions comparison between measurement and calculations for the power channel, case 1a.

Table 5. Filter parameters for Case Study 1.

	Case 1a	Case 1b
$\bar{Z}_p$	$L_p = 9\,\mu\text{H}, C_p = 8.27\,\text{nF}$	$L_p = 41\,\mu\text{H}, C_p = 1.72\,\text{nF}$
$\bar{Z}_s$	$L_s = 41\,\mu\text{H}, C_s = 1.72\,\text{nF}$	$L_s = 9\,\mu\text{H}, C_s = 8.27\,\text{nF}$

For the same circuit (data between outer coils), a comparison between analytical calculations and measurement have been performed, and shown in Figure 10; in this case we notice again a peak reduction and a slight frequency shifting phenomenon. Both phenomena are due, also in this case, to the tolerances and non-ideality of the components. The selection of higher quality components and a sensitivity study (performed for instance with MonteCarlo analysis as in [9]) could be useful for a more accurate realization of the system.
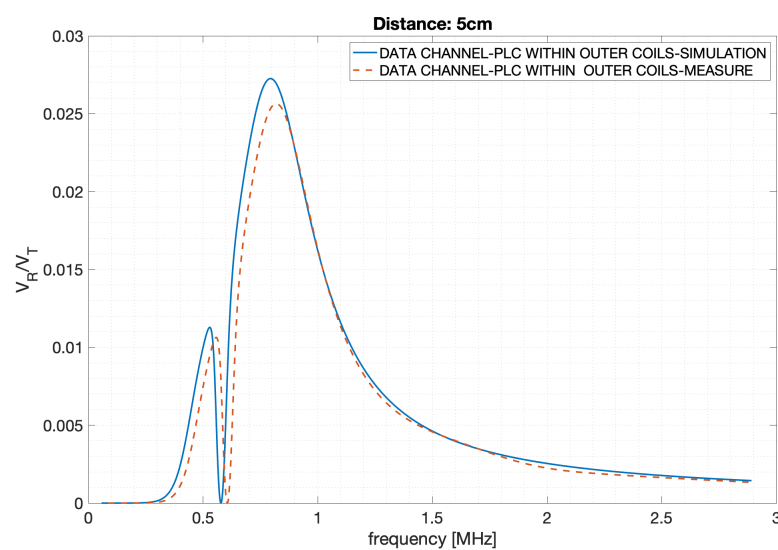

Figure 10. Transfer Functions comparison between measurement and calculations for the data channel, case 1a.

As shown in the previous figures, the designed system performs as desired; for this reason the following figures only show analytical results.

Figure 11 shows the analytical results relative to the power transfer function for the two circuits (data from inner and outer coils), each of them implemented with the different filters as reported in Table 5, resulting in a total number of simulations equal to four. In particular, Figure 11 shows that using the inner coils for data transfer leads to a slightly narrower power channel with respect to the use of outer coils; in addition, different implementation of the filters can enhance or reduce this behavior.
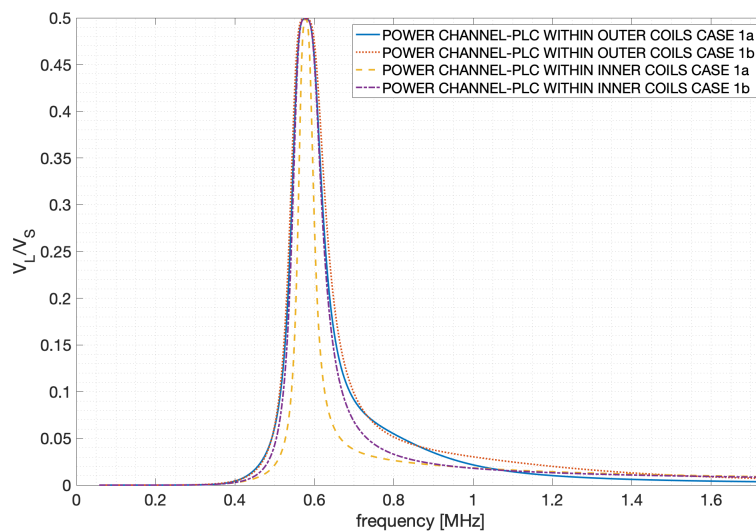
Figure 11. Transfer function comparison for the power channel, Case Study 1.

Figure 12 shows the analytical results relative to the data transfer function for the two circuits (data from inner and outer coils), each of them implemented with the different filters as reported in Table 5. The different behaviors of the transfer functions relative to the data channel are now extremely evident and it is not only reduced to a slight difference in the bandwidth. In particular, there is a strong effect on the transfer function both of the different data access point and filter realization. In particular, the best performing solution in terms of bandwidth consists in the use of inner coils with the series filters implemented as $L_s = L_2$ and $C_s = C_2$, while the worst solution consists in the use of outer coils with the parallel filters implemented as $L_p = L_2$ and $C_p = C_2$.
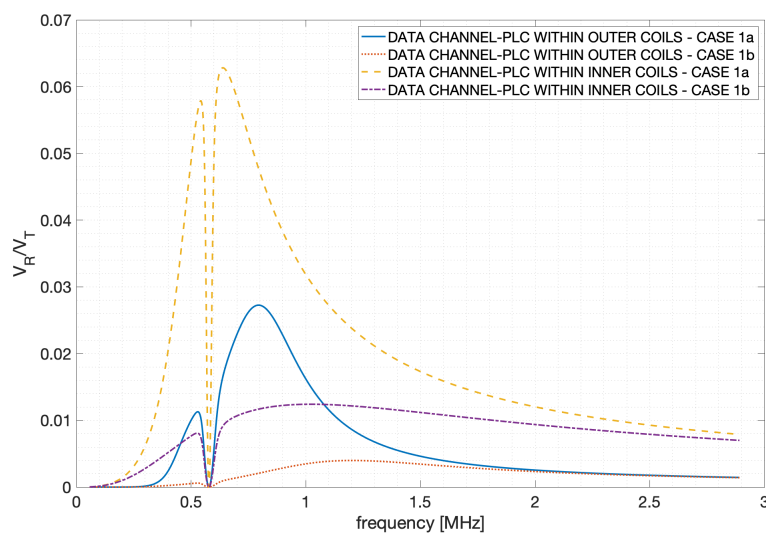

Figure 12. Transfer function comparison for the data channel, Case Study 1.

This qualitative analysis is validated by the calculation of the channel capacity in the four previous cases. We can refer to the Shannon-Hartley approach: the signal sent from the transmitter is filtered by the channel transfer's function, which is in general selective and reaches the receiver together with the noise which, in this case, is mainly produced by the signal generator and RF amplifier. The following Shannon-Hartley law can be used:

$$C = \int_0^B \log_2 \left(1 + \frac{S(f)}{N(f)}\right) df \tag{8}$$

in which C is the channel capacity in bits per second, B is the bandwidth of the channel, $S(f)$ is the signal power spectrum, $N(f)$ is the noise power spectrum and f is the frequency. As for the channel capacity objective, the following assumptions are made: both the injected power spectrum $S_I(f) = S_I$, and the noise power spectrum $N(f) = N$, are frequency independent, and the noise is considered as additive white Gaussian noise at the receiver. The SNR is then defined as $SNR = S_I/N$, and the received power spectrum can be expressed as a function of the injected power spectrum and the transfer function, according to $S(f) = \|H(f)\|^2 S_I$. Under these assumptions, (8) can be rewritten as

$$C = \int_0^B \log_2 \left(1 + \|H(f)\|^2 SNR\right) df \tag{9}$$

Figure 13 shows the channel capacity in the frequency band $[10kHz, 30MHz]$, typical of broadband power line. It is evident that reasonable data transmission capacity can be obtained for a 5 cm distance, and that for high signal to noise ratio a speed of above 1Mbit per second can be reached. In addition, as qualitatively seen from the transfer functions, the data communication between inner coils is outperforming other practical solutions.
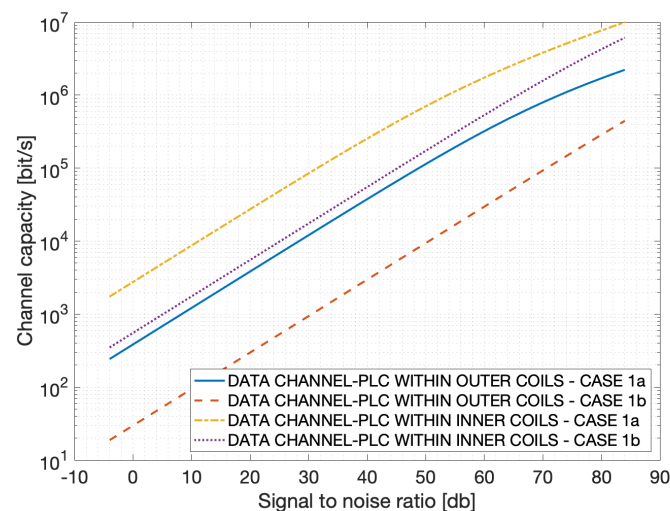

Figure 13. Channel capacity comparison, Case Study 1.

5.3. Case Study 2 (15 cm Distance)

For the Case Study 2 (15 cm distance), the following table resumes the filter parameters for the subcases (a) and (b) (as a matter of fact, the filters are the same used for Case Study 1).

For the sake of conciseness, relative to Case Study 2, we show the comparison between analytical results and simulation only for the data transfer between outer coils, as reported in Figure 14. In this case we notice again a peak reduction and a slight frequency shifting phenomenon due to components characteristics.
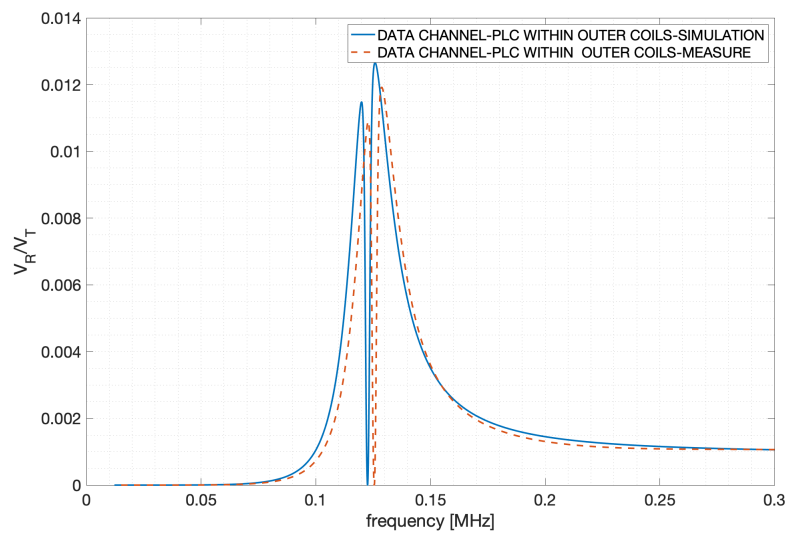
Figure 14. Transfer function comparison between measurement and calculations for the data channel, case 2a.

Figure 15 shows the analytical results relative to the power transfer function for the two circuits (data from inner and outer coils), each of them implemented with the different filters as reported in Table 6. As happened for Case Study 1, it can be noticed that the use of the inner coils for data transfer leads to a slightly narrower band of the power channel with respect to the use of outer coils. In addition, a reduction of the peak value (transfer efficiency) is observed, and it is due to the increased distance: only in the case of an ideal system without parasitic resistances can maximum transfer ($S_{21} = 1$) be achieved; in realistic cases at increasing distances there will always be a decreasing efficiency.
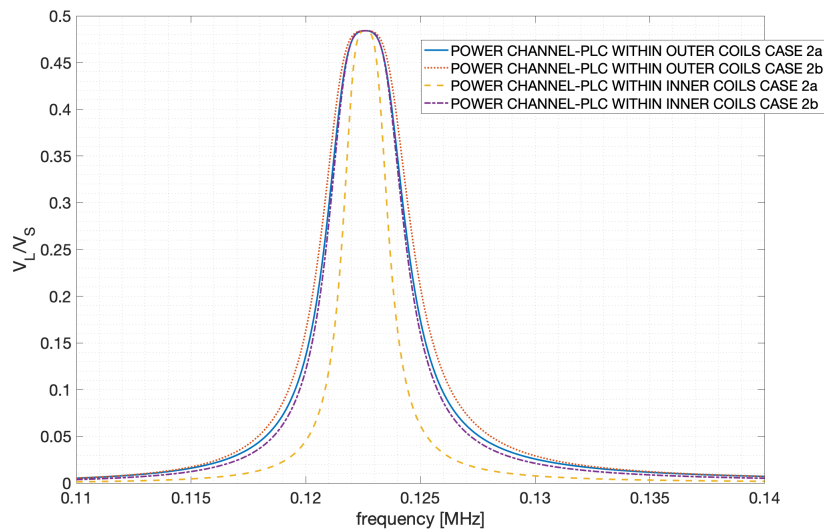

Figure 15. Transfer function comparison for the power channel, Case Study 2.

Table 6. Filter parameters for Case Study 2.

	Case 2a	Case 2b
$\bar{Z}_p$	$L_p = 9\,\mu\text{H},\ C_p = 8.27\,\text{nF}$	$L_p = 41\,\mu\text{H},\ C_p = 1.72\,\text{nF}$
$\bar{Z}_s$	$L_s = 41\,\mu\text{H},\ C_s = 1.72\,\text{nF}$	$L_s = 9\,\mu\text{H},\ C_s = 8.27\,\text{nF}$

Figure 16 shows the analytical results relative to the data transfer function for the two circuits (data from inner and outer coils), each of them implemented with the different filters as reported in Table 6. Looking at the graphs from a qualitative point of view, the two best performing solutions (in terms of bandwidth) seem to be the ones in which data is transferred either between inner or outer coils with the filters (either parallel or series) implemented as in case 2a (i.e., with the filters elements L and C having the same values as the coils'inductance and resonance capacitors). However data with outer coils with filters a) have a narrow bandwidth centred on the notch, giving selectivity that is not suitable for data transmission.
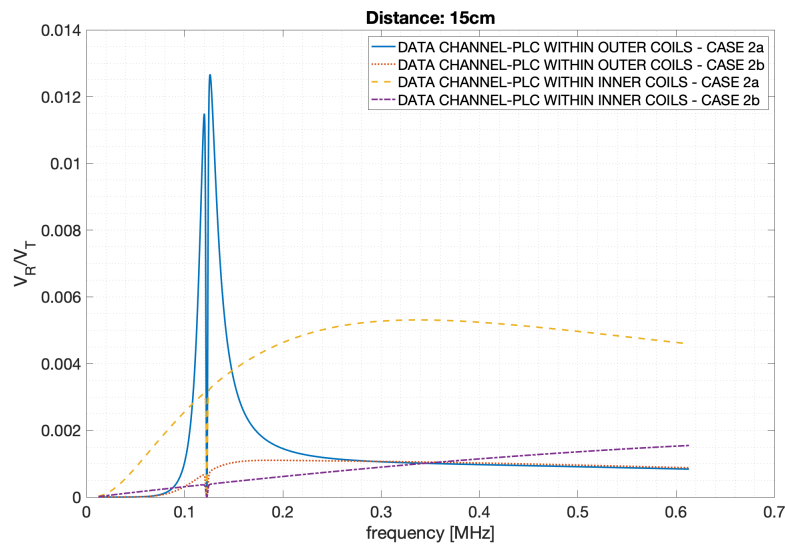

Figure 16. Transfer function comparison for the data channel, Case Study 2.

Figure 17 shows the channel capacity for Case Study 2. This case study, characterized by a higher distance, shows a lower data transmission capacity if compared to Case Study 1, however the system performances could be more than acceptable depending on the specific application. Also in this case the data transfer between inner coils is outperforming other practical solutions.
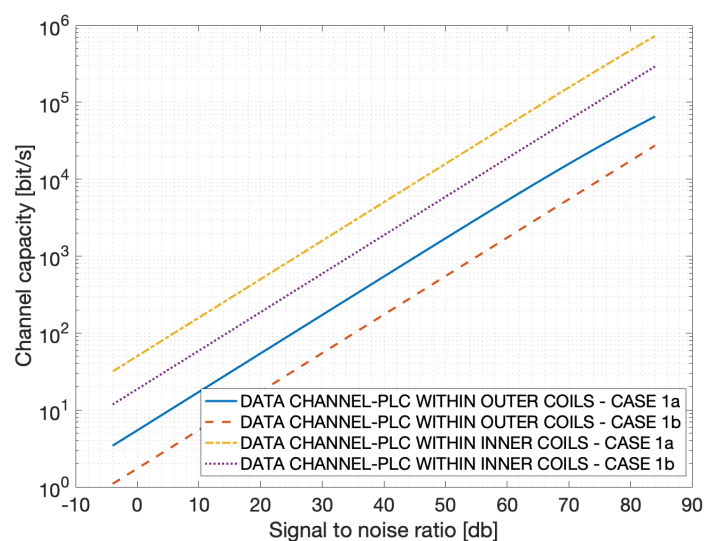

Figure 17. Channel capacity comparison, Case Study 2.

5.4. Discussion

The measurements and calculations shown before can be used to draw the following considerations relative to the combined system allowing both power and data transfer wirelessly and guaranteeing an efficient interface with a PLC system.

(a)   If the power section is properly designed in order to guarantee the desired power at the receiver (i.e., maximum power, maximum energy efficiency or an intermediate situation), the presence of additional filters for data transfer does not affect power at the resonant frequency.

(b)   The convenience of using different access points for data and power (data from inner coils) is influenced by the realization of the filters. From our analysis, data access from inner coils is convenient in terms of data bandwidth, provided that the proper series filter on the inner coils is designed.

(c)   From our analysis, higher data bandwidth from inner coils (the most convenient approach) results in an increased selectivity of the power channel.

(d)   It is known that PLC works well with attenuations that can reach up to -40 db, that corresponds to a voltage gain of 10^{-2}. As for the injected power of typical PLC systems, the usual SNR is in the order of 60 db, leading to the more than acceptable capacities shown in the graphs.

Point (a) is valid if the filters' components are selected with a high accuracy, something that will also prevent frequency shifting that reduces the system's efficiency, especially thinking about point (c). The consideration of point (b) is valid based on the results obtained using basic $L - C$ filters. The particular choice of the values the L and C filters components has been performed for the sake of simplicity. In basic second order LC filters, the same resonant frequency can be obtained (theoretically) with an infinite combination of components, and when power is transmitted additional constraints on the components obviously arise. Furthermore, components dimension should also be taken into account in the design process, for instance speaking about higher value inductances.

Higher order filters will be the object of future investigations, since their use should be able to increase the system's performance, especially from the data transfer point of view. The series and parallel filters discussed in the paper perform the operation that PLC couplers perform in commercial modems, i.e., impedance matching to achieve efficient data transfer and prevent power to damage the modem itself.

Higher order filters are generally used in PLC modems and can be properly designed for this specific system; a sentence regarding higher order filters is already present in Section 5, but it has now been extended.

As a final consideration, the use of different access points for data and power can be of interest when a higher data bandwidth must be achieved, and when galvanic insulation between the power system and data modem is needed. In these cases, the cost of specific filters should be evaluated in order to obtain the desired performances.

6. Conclusions

In this paper the authors show that a combined WPT-PLC system (retaining both the usefulness of transmitting power without electrical contact and the possibility of being included in a power line communication environment) can achieve both power efficiency and high channel capacity. In addition, a multiple coils system (which is used to increase power transmission distance with respect to a two coils system) can be exploited as a multiple access point, reaching higher data transfer capacity. In the paper, the authors analyze and measure different setups, showing that the proper design of the coupling filters is the key point to achieve higher data transfer bandwidth, and in this case different access points can give better results.

Conflicts of Interest: The authors declare no conflict of interest.

Appendix A

Appendix A.1

The transfer function $\dot{V}_L/\dot{V}_S$ relative to the power transfer for the system reported in Figure 2 can be calculated as follows; the parallel filter $\bar{Z}_p$ is composed by a parallel connection between an inductor L_p and a capacitor C_p.

$$\frac{\dot{V}_L}{\dot{V}_S} = R_L \frac{j\omega^3 k_{12}k_{23}k_{34}L_2L_3\sqrt{L_1L_4}}{A\omega^4 + B\omega^2 + C} \frac{\bar{Z}_p + R_T}{\bar{Z}_p + R_S + R_T}\bar{Z}_{p4} \tag{A1}$$

with

$$\bar{Z}_p = \frac{j\omega L_p}{1 - \omega^2 L_p C_p}$$

$$\bar{Z}_{p4} = \frac{(\bar{Z}_p + R_R)R_L}{\bar{Z}_p + R_R + R_L}$$

$$\bar{Z}_{th} = \frac{(\bar{Z}_p + R_T)R_S}{\bar{Z}_p + R_T + R_S}$$

$$A = k_{12}^2 k_{34}^2 L_1 L_2 L_3 L_4$$

$$B = k_{12}^2 L_1 L_2 \bar{Z}_3 \bar{Z}_4 + k_{23}^2 L_2 L_3 \bar{Z}_1 \bar{Z}_4 + k_{34}^2 L_3 L_4 \bar{Z}_1 \bar{Z}_2 \tag{A2}$$

$$C = \bar{Z}_1 \bar{Z}_2 \bar{Z}_3 \bar{Z}_4$$

$$\bar{Z}_1 = \bar{Z}_{th} + R_{p1} + j\omega L_1 - \frac{j}{\omega C_1}$$

$$\bar{Z}_2 = R_{p2} + j\omega L_2 - \frac{j}{\omega C_2}$$

$$\bar{Z}_3 = R_{p3} + j\omega L_3 - \frac{j}{\omega C_3}$$

$$\bar{Z}_4 = \bar{Z}_{p4} + R_{p4} + R_L + j\omega L_4 - \frac{j}{\omega C_4},$$

The transfer function $\dot{V}_R/\dot{V}_T$ relative to the data transfer for the system reported in Figure 2 is

$$\frac{\dot{V}_R}{\dot{V}_T} = \frac{j\omega^3 k_{12}k_{23}k_{34}L_2L_3\sqrt{L_1L_4}}{A\omega^4 + B\omega^2 + C} \frac{R_R R_L R_S}{(R_R + R_L + \bar{Z}_p)(R_S + R_t + \bar{Z}_p)} \tag{A3}$$

with

$$\bar{Z}_p = \frac{j\omega L_p}{1 - \omega^2 L_p C_p}$$

$$\bar{Z}_{p4} = \frac{(\bar{Z}_p + R_R)R_L}{\bar{Z}_p + R_R + R_L}$$

$$\bar{Z}_{th} = \frac{(\bar{Z}_p + R_T)R_S}{\bar{Z}_p + R_T + R_S}$$

$$A = k_{12}^2 k_{34}^2 L_1 L_2 L_3 L_4$$

$$B = k_{12}^2 L_1 L_2 \bar{Z}_3 \bar{Z}_4 + k_{23}^2 L_2 L_3 \bar{Z}_1 \bar{Z}_4 + k_{34}^2 L_3 L_4 \bar{Z}_1 \bar{Z}_2$$

$$C = \bar{Z}_1 \bar{Z}_2 \bar{Z}_3 \bar{Z}_4$$

$$\bar{Z}_1 = \bar{Z}_{th} + R_{p1} + j\omega L_1 - \frac{j}{\omega C_1}$$

$$\bar{Z}_2 = R_{p2} + j\omega L_2 - \frac{j}{\omega C_2}$$

$$\bar{Z}_3 = R_{p3} + j\omega L_3 - \frac{j}{\omega C_3}$$

$$\bar{Z}_4 = \bar{Z}_{p4} + R_{p4} + R_L + j\omega L_4 - \frac{j}{\omega C_4},$$

(A4)

Appendix A.2

The transfer function $\dot{V}_L/\dot{V}_S$ relative to the power transfer for the system reported in Figure 3 is calculated as follows, in which the series filter $\bar{Z}_s$ is composed by a series connection between an inductor L_s and a capacitor C_s.

$$\frac{\dot{V}_L}{\dot{V}_S} = R_L \frac{j\omega^3 k_{12} k_{23} k_{34} L_2 L_3 \sqrt{L_1 L_4}}{A\omega^4 + B\omega^2 + C},$$

(A5)

$$A = k_{12}^2 k_{34}^2 L_1 L_2 L_3 L_4$$

$$B = k_{12}^2 L_1 L_2 \bar{Z}_3 \bar{Z}_4 + k_{23}^2 L_2 L_3 \bar{Z}_1 \bar{Z}_4 + k_{34}^2 L_3 L_4 \bar{Z}_1 \bar{Z}_2$$

$$C = \bar{Z}_1 \bar{Z}_2 \bar{Z}_3 \bar{Z}_4$$

$$\bar{Z}_s = j\left(\omega L_s - \frac{1}{\omega C_S}\right)$$

$$\bar{Z}_{p2} = \frac{R_T \bar{Z}_s}{R_T + \bar{Z}_s}$$

$$\bar{Z}_{p3} = \frac{R_R \bar{Z}_s}{R_R + \bar{Z}_s}$$

$$\bar{Z}_1 = R_{p1} + R_S + j\omega L_1 - \frac{j}{\omega C_1}$$

$$\bar{Z}_2 = R_{p2} + j\omega L_2 - \frac{j}{\omega C_2} + \bar{Z}_{p2}$$

$$\bar{Z}_3 = R_{p3} + j\omega L_3 - \frac{j}{\omega C_3} + \bar{Z}_{p3}$$

$$\bar{Z}_4 = R_{p4} + R_L + j\omega L_4 - \frac{j}{\omega C_4},$$

(A6)

The transfer function $\dot{V}_R/\dot{V}_T$ relative to the data transfer for the system reported in Figure 3 is

$$\frac{\dot{V}_R}{\dot{V}_T} = R_R \frac{j\omega k_{23}\bar{Z}_1\bar{Z}_4\sqrt{L_2 L_3}}{A\omega^4 + B\omega^2 + C} \frac{\bar{Z}_{p3}\bar{Z}_S}{R_T + \bar{Z}_S} \tag{A7}$$

with

$$
\begin{aligned}
\bar{Z}_s &= j\left(\omega L_s - \frac{1}{\omega C_S}\right) \\
\bar{Z}_{p2} &= \frac{R_T \bar{Z}_s}{R_T + \bar{Z}_s} \\
\bar{Z}_{p3} &= \frac{R_R \bar{Z}_s}{R_R + \bar{Z}_s} \\
\bar{Z}_{2b} &= R_{p2} + R_T + j\omega L_2 - \frac{j}{\omega C_2} + \bar{Z}_{p2} \\
\bar{Z}_{3b} &= R_{p3} + R_S + j\omega L_3 - \frac{j}{\omega C_3} + \bar{Z}_{p3}
\end{aligned}
\tag{A8}
$$

References

1. Kurs, A.; Karalis, A.; Moffatt, R.; Joannopoulos, J.; Fisher, P.; Soljacic, M. Wireless power transfer via strongly coupled magnetic resonances. *Science* **2007**, *317*, 83-86. [CrossRef] [PubMed]
2. Lee, S.H.; Lorenz, R.D. Development and Validation of Model for 95%-Efficiency 220-W Wireless Power Transfer Over a 30-cm Air Gap. *IEEE Trans. Ind. Appl.* **2011**, *47*, 2495–2504. [CrossRef]
3. Madawala, U.K.; Thrimawithana, D.J. A Bidirectional Inductive Power Interface for Electric Vehicles in V2G Systems. *IEEE Trans. Ind. Electron.* **2011**, *56*, 4789–4796. [CrossRef]
4. Barmada, B.; Tucci, M.; Raugi, M.; Maryanka, Y.; Amrani, O. PLC Systems for Electric Vehicles and Smart Grid Applications. In Proceedings of the IEEE International Symposium of Powerline Communications and its Applications (ISPLC), Johannesburg, South Africa, 24–27 March 2013; pp. 23–28.
5. Lienard, M.; Carrion, M.; Degardin, V.; Degauque, P. Modeling and Analysis of In-Vehicle Power Line Communication Channels. *IEEE Trans. Veh. Technol.* **2008**, *57*, 670–679. [CrossRef]
6. Mohammadi, M.; Lampe, L.; Lok, M.; Mirabbasi, S.; Mirvakili, M.; Rosales, R.; van Veen, P. Measurement Study and Transmission for In-vehicle Power Line Communication. In Proceedings of the IEEE International Symposium of Powerline Communications and Its Applications (ISPLC), Dresden, Germany, 29 March–1 April 2009; pp. 73–78.
7. Barmada, S.; Raugi, M.; Tucci, M. Power line communication integrated in a Wireless Power Transfer system: A feasibility study. In Proceedings of the IEEE International Symposium of Powerline Communications and Its Applications (ISPLC), Glasgow, UK, 30 March–2 April 2014; pp. 116–120.
8. Barmada, S.; Tucci, M. Optimization of a Magnetically Coupled Resonators System for Power Line Communication Integration. In Proceedings of the IEEE Wireless Power Transfer Conference (WPTC), Boulder, CO, USA, 13–15 May 2015; pp. 1–4.
9. Barmada, S.; Dionigi, M.; Mezzanotte, P.; Tucci, M. Design and Experimental Characterization of a Combined WPT-PLC System. *Wirel. Power Transf.* **2017**, *4*, 160–170. [CrossRef]
10. Lu, Y.; Ma, D.B. Wireless Power Transfer System Architectures for Portable or Implantable Applications. *Energies* **2016**, *9*, 1087. [CrossRef]
11. Wang, Z.; Wei, X.; Dai, H. Design and Control of a 3 kW Wireless Power Transfer System for Electric Vehicles. *Energies* **2016**, *9*, 10. [CrossRef]
12. Ouannes, I.; Nickel, P.; Dostert, K. Cell-wise monitoring of lithium ion batteries for automotive traction applications by using power line communication: Battery modeling and channel characterization. In Proceedings of the IEEE International Symposium of Powerline Communications and Its Applications (ISPLC), Glasgow, UK, 30 March–2 April 2014; pp. 24–29.
13. Son, Y.; Pulkkinen, T.; Moon, K.; Kim, C. Home Energy Management System Based on Power Line Communication. *IEEE Trans. Cons. Electron.* **2010**, *56*, 1380–1386. [CrossRef]
14. Barmada, S.; Tucci, M. Analysis of Two/Four Coils WPT Systems for Embedded PLC Communications. *Appl. Comput. Electromagn. Soc. J.* **2018**, *33*, 1112–1116.

15. Sample, A.P.; Meyer, D.A.; Smith, J.R. Analysis, Experimental Results and Range Adaptation of Magnetically Coupled Resonators for Wireless Power Transfer. *IEEE Trans. Ind. Electron.* **2011**, *58*, 544–554. [CrossRef]

16. Wheeler, H.A. Simple inductance formulas for radio coils. *Proc. Inst. Radio Eng.* **1928**, *16*, 1398–1400. [CrossRef]

17. Grandi, G.; Kazimierczuk, M.K.; Massarini, A.; Reggiani, U. Stray Capacitances of Single-Layer Solenoid Air-Core Inductors. *IEEE Trans. Ind. Appl.* **1999**, *35*, 1162–1168. [CrossRef]

18. Grover, F.W. *Inductance Calculation: Working Formulas and Tables*; Dover Publications, Inc.: New York, NY, USA, 1946.

19. Cheon, S.; Kim, Y.H.; Kang, S.Y.; Lee, M.L.; Lee, J.M.; Zyung, T. Circuit-Model-Based Analysis of a Wireless Energy-Transfer System via Coupled Magnetic Resonances. *IEEE Trans. Ind. Electron.* **2010**, *58*, 2906–2914. [CrossRef]